

A Simple Ball Averager for Reference Sphere Calibrations

Ulf Griesmann, Quandou Wang, Johannes Soons, and Remi Carakos

National Institute of Standards and Technology (NIST), Manufacturing Engineering Laboratory,
Gaithersburg, MD 20899-8223, U.S.A.

ABSTRACT

When measuring the form errors of precision optics with an interferometer, calibration of the reference wavefront is of central importance. In recent years, ball averaging, or random ball testing, has emerged as a robust method for calibrating spherical reference wavefronts in converging beams. We describe a simple instrument, consisting of an air bearing and two electric motors, that can rotate the test ball around three axes as required for a ball averaging test. The performance of the instrument is demonstrated by using it to calibrate a concave transmission sphere. Further we discuss the effects of image sampling at random locations or on uniform grids, and the effect of correlated measurements. Finally, we describe a method to determine the number of measurements which are sufficient for a ball averaging calibration.

Keywords: Interferometry, reference wavefront calibration, transmission sphere, ball averaging test

1. INTRODUCTION

Interferometers with spherical test wavefronts are used in the metrology of spherical and, in conjunction with refractive or diffractive null-optics, aspheric surfaces. The calibration of the reference surface is a critical step in the measurement of parts with form errors that may be of similar magnitude than the departure from the perfect spherical form of the reference wavefront. Multi-position tests for the calibration of spherical reference surfaces are well established. In the simplest form, three measurement positions of two spheres are required, one of which must be a transmission sphere.¹⁻⁴ This two-sphere test requires that one of the spheres be rotated about the optical axis of the interferometer, which is difficult to accomplish in practical realizations of the test. Selberg⁵ described an extension of the two-sphere test with five positions which eliminates the effect of misalignment between the axis of rotation and the optical axis. Analogs of three-flat tests for flat calibrations using three spherical surfaces are also described in the literature.⁶ The calibration of concave transmission spheres for Fizeau interferometers with spherical wavefronts is of particular importance because this type of test objective is almost universally used in optics shops for the measurement of spherical surfaces. Concave transmission spheres, or indeed any measurement objective that creates a spherical test wavefront with a converging beam, can be calibrated with the method of ball averaging. This method appears to have first been described by Parks et al.⁷ A ball is set up confocal with the light cone of the test objective, as indicated in Fig. 1. For an ideal interferometer, one which does not suffer from coherent stray reflections and other imperfections, the measured wavefront W_n is a superposition of the wave reflected by the reference surface, W^R , and the wave W_n^B reflected from the ball:

$$W_n = W^R + W_n^B. \quad (1)$$

The index n denotes one of many orientations in which the ball is measured. The wavefront reflected by the ball, W_n^B , is twice the form error of the ball surface S_n^B :

$$W_n^B = 2S_n^B. \quad (2)$$

The recipe for the ball averaging method is to average many measurements of the ball in different orientations against a reference surface. For N measurements the resulting wavefront \overline{W} is:

$$\overline{W} = \frac{1}{N} \sum_{n=1}^N W_n = \frac{1}{N} \sum_{n=1}^N (W^R + W_n^B) = W^R + \frac{1}{N} \sum_{n=1}^N W_n^B = W^R + \frac{2}{N} \sum_{n=1}^N S_n^B. \quad (3)$$

\overline{W} is the sum of the desired reference wavefront W^R and the arithmetic mean of all ball area measurements and any noise. The behavior of this mean on the right side of Eq. (3) is easiest to understand if it is assumed that the interferometer camera

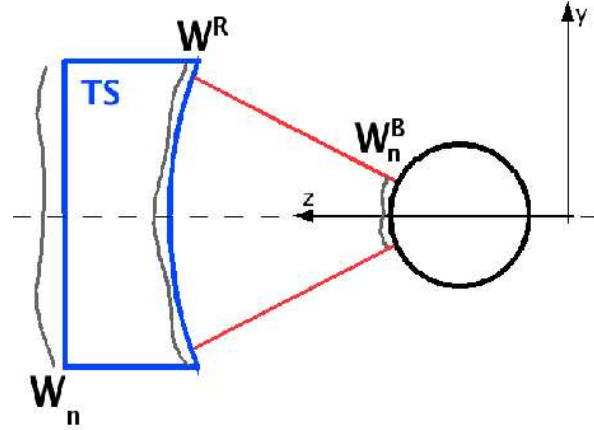


Figure 1. Concept of the ball averaging test for the calibration of a concave transmission sphere (TS). W^R is the wavefront of the light field reflected by the spherical reference surface, W_n^B is the wavefront of the light field reflected off the ball in orientation n . W_n denotes the superposition of the test- and reference waves.

has only one pixel. S^B represents the form error of the ball defined as the departure from the best-fit sphere. Rotating the ball at random, making repeated measurements of the form error, and then averaging the results collectively, amounts to a Monte-Carlo integration of the form error S^B over the entire ball surface. Since the integral of the form error, when integrated over the whole surface, must be zero we have:

$$\lim_{N \rightarrow \infty} \left(\frac{1}{N} \sum_{n=1}^N W_n^B \right) = 0, \quad (4)$$

and the averaged measurements \overline{W} in Eq. (3) converge to the reference wavefront W^R . Assuming that the W_n^B are uncorrelated samples from a distribution with zero mean, the root-mean-square (RMS) of the mean in Eq. (4) will be proportional to $1/\sqrt{N}$. In a practical realization of the ball averaging test, the conditions just described for the integration of the ball form error S^B are never perfectly realized. Because an interferometer measures S^B not at a single point but over an area, the measurement areas will tend to overlap as the number N of measurements increases, which is a possible cause of correlations in the sampling, especially when images are not rotated about the optical axis. It is also not true that the measured S^B represents the form error with respect to the best fit sphere for the whole ball surface; it only represents the departure from the local best fit sphere. Nonetheless, computer simulations (see section 3) suggests that Eq. (4) holds true in the presence of the imperfections encountered in practical realizations of the test. The remaining question to be answered is: how many measurements must be made to obtain a good calibration of the reference wavefront W^R ? We will return to this question at the end of this article.

2. BALL MANIPULATOR DESIGN

2.1. Mechanical Design

As described by Parks et al.,⁷ the ball averaging test can be implemented by setting the ball on a three-point mount and rotating it manually after each phase measurement. This has obvious disadvantages. The operator must touch the ball briefly, which will change the temperature of the ball at some locations and cause changes in the shape of the ball unless it is made from a material with a very low coefficient of thermal expansion. Touching the ball also makes it likely that it is contaminated either with dust or residues present on the gloved hands of the operator. Another problem is a potential bias in the calibration because the operator has no way of knowing if the measurement locations represent a fair random sample. One must also consider that the tedium of manual calibration may predispose the operator to make too few measurements. For these reasons, a ball manipulator that automates the measurement procedure is highly desirable.

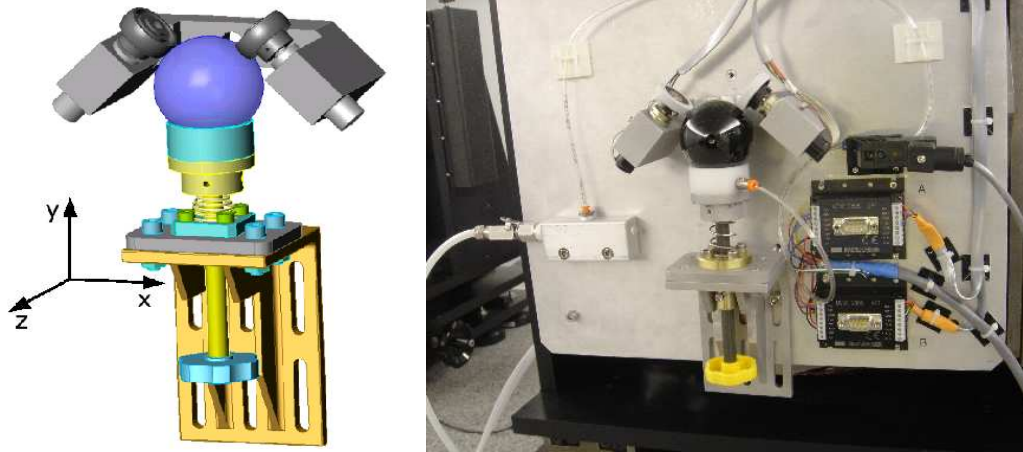


Figure 2. Solid model of ball manipulator (left) and actual implementation (right). z indicates the direction of the optical axis of the interferometer. The ball is made from an opaque filter glass. It has a diameter of 50 mm. To the right of the ball mount one can see two motion controllers and a solenoid valve which is used to switch the air flow to the air bearing.

A solid model of a prototype ball manipulator developed at the National Institute of Standards and Technology (NIST) is shown on the left side of Fig. 2. On the right side of Fig. 2 is a photograph of the actual manipulator used with NIST’s “eXtremely accurate CALIBration InterferometerR” (XCALIBIR). The ball is made from Schott UG-1 filter glass*. An opaque glass must be used to avoid a coherent reflection from the “back” surface of the ball. The diameter of the ball is 50 mm. The ball is located by a spherical air bearing, made from a hard plastic material, with a diamond-turned bearing surface which matches the radius of the ball. Air is supplied to the bearing through six small nozzles which are arranged symmetrically in the air bearing surface. Air flow to the bearing is activated with a solenoid valve whenever the ball is rotated but remains switched off during measurements. The air bearing is mounted on a spring loaded shaft in a linear ball bearing which can be clamped in place. This makes it easy to place the ball into the air bearing and the spring also ensures a reproducible force of the driver wheels onto the ball surface. Two driver wheels, driven by small electrical motors, are used to rotate the ball. In its most general form, the ball averaging test requires that it be possible to bring an arbitrary point on the sphere onto the optical axis of the interferometer. Additionally, it must also be possible to arbitrarily rotate the area that is illuminated by the interferometer around the optical axis. It follows that the manipulator must be able to rotate the ball about all three axes shown in Fig. 2. To effect a rotation about the x -axis, both driver wheels are rotated with the same angular velocity in the same direction. When the motors are rotated in opposite directions, but with equal magnitude of angular velocity, the ball will rotate around the vertical y -axis. A rotation around the z -axis, the optical axis of the interferometer, is slightly more difficult to accomplish. The ball is first rotated by -90° around the x -axis which brings the point on the z -axis to the “top”. Then the ball is rotated around the y -axis by the desired angle, and finally the ball is rotated around the x -axis by $+90^\circ$ to bring the point at the “top” back onto the z -axis. The rotations about the x - and y -axes were calibrated using a temporary fiducial mark on the ball. We determined a standard positioning uncertainty of 0.5° for a rotation of 360° . The positioning uncertainty is approximately proportional to the rotation angle.

2.2. Choosing Points

The motorized ball manipulator can be used to investigate different strategies for sampling the ball surface. We have investigated two strategies for choosing sampling locations on the ball. In the first, a random point on the ball surface is chosen using an algorithm described by Weisstein⁸ for calculating random points on a sphere with uniform probability density. The ball is then rotated to bring this point onto the optical axis ($x = y = 0$), with a random orientation about the z axis, and a form error measurement is made. With this strategy some measurements contain a large overlap as can be seen in the simulations in section 3. Because the measurements are no longer uncorrelated when they overlap, it can be argued

*Certain commercial equipment, instruments, or materials are identified in this document. Such identification does not imply recommendation or endorsement by the National Institute of Standards and Technology, nor does it imply that the products are identified are necessarily the best available for the purpose.

that this violates one of the assumptions of the ball averaging test which may reduce the effectiveness of the calibration method. This effect is reduced by image rotations (see section 3). To investigate whether different sampling strategies lead to differences in the convergence of the test, we have used a second strategy for picking measurement locations by distributing the locations uniformly over the ball. An algorithm capable of distributing an arbitrary number of measurement locations was described by Saff and Kuijlaars.⁹ In this algorithm the points are distributed along a spiral that starts at one pole of the sphere and ends at the other and generates points which are approximately uniformly distributed.

2.3. A Note on Dynamic Calibration

The ball manipulator described in section 2.1 may be used for a dynamic version of the ball averaging test in which the driver wheels that rotate the ball (see Fig. 2) are removed and the ball rotates in the air bearing during the measurements. When the air supply is turned on, the unrestrained ball will begin to rotate because small differences in the air nozzles cause an uneven distribution of forces acting on the ball in the bearing. One could imagine having additional nozzles which are individually switchable to help randomize the motion of the ball. It is important that the principal moments of inertia of the ball are identical, otherwise the ball will wobble in the bearing. The ball may also settle into a non-random motion pattern which leads to sampling of the ball surface with non-uniform probability density and an undesirable bias in the calibration of the reference wavefront W^R . A more elaborate dynamic ball averaging tester has been described in the patent literature by Evans et al.¹⁰

3. SIMULATION

We simulated the ball averaging test to gain some insight into the convergence of the mean in Eq. (4). A ball with a smooth sphericity error was modelled using a number of low-order spherical harmonic functions. This ball is shown in Fig. 3. The reference wavefront was assumed to be perfect and thus $W^R = 0$. Sampling strategies with random and uniform sample locations were investigated. The sampling locations for these strategies are shown in Figs. 4, 5, and 6. Fig. 4 represents measurements at random locations on the sphere with uniform probability density. Each circle indicates a measurement but the circular area does not represent the entire measurement area. The measurement area in the simulation is identical to the area imaged by a NA=0.39 (f/1.3) measurement objective. The angular orientation of the circular measurement areas about their centers was also randomized. It is indicated by a radial line in Figs. 4, 5, and 6. In the ball averaging tests, trial runs of up to 4096 measurements were simulated. Each trial was repeated 20 times to calculate the repeatability for the sum term in Eqs. (3) and (4). In the case of the uniform sampling locations (Fig. 5), the ball was rotated at random before each sampling sequence to ensure that different locations are sampled during each test. The results of the computer simulated ball averaging tests are in the graphs on the right side of Figs. 4, 5, and 6. In the figures, the root-mean-square (RMS) of the sample averages are plotted against the number of measurements. Each red dot represents an independent trial with the stated number of samples. Red lines indicate the average of the RMS values of the various trials and their repeatability with a coverage factor of 2. To calculate the solid blue line, the RMS for each sample from all trials was computed and the arithmetic mean of these was calculated which is the value of the solid blue graph for $N = 1$. This was then multiplied with $1/\sqrt{N}$ to obtain the values of the graph for $N > 1$. The dashed blue lines indicate the repeatability of the RMS values calculated at $N = 1$ and scaled with $1/\sqrt{N}$. A large variance in RMS values of individual images results in a wider uncertainty zone requiring more measurements. Figs. 4 and 5 show that, independent of sampling strategy, both curves converge to zero, the assumed error of the reference wavefront. In both cases the convergence closely follows a $1/\sqrt{N}$ law. The behavior of these sampling strategies for more complex form errors of the ball remains to be investigated. We find that the convergence no longer follows $1/\sqrt{N}$ when the orientation of the measurement areas is not varied. In Fig. 6 the measurement locations are chosen at random but the orientation of the measurement areas remains fixed. For large numbers of averaged measurements the RMS of the mean is significantly larger than the expected $1/\sqrt{N}$ behavior which underscores the need for proper variation of measurement areas in both orientation and location.

4. A CALIBRATION EXAMPLE

Using the XCALIBIR interferometer at NIST, the ball manipulator described in section 2 was put to the test by calibrating the form error of a 300 mm concave transmission sphere with NA=0.39 (f/1.3). Three sampling strategies, random sampling, uniform sampling, and random sampling with random orientation of the measurement area, using 100 measurements for each case, were investigated. Alignment errors, tilt and defocus, were subtracted numerically from all measurements before averaging the measurements. The resulting estimate of the reference wavefront W^R is shown in Fig. 7. Unlike

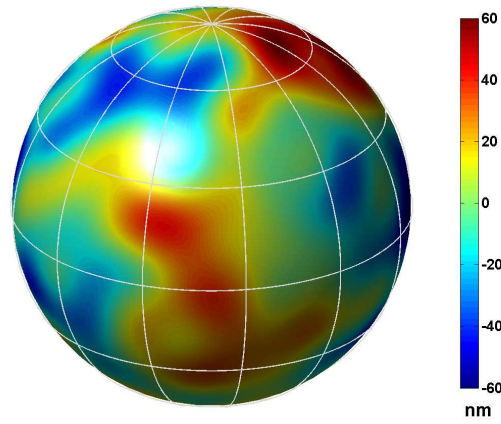


Figure 3. Computer simulated ball with a sphericity error of 120 nm ($\lambda/5$ at $\lambda=633$ nm) which is close to the form error of the black glass ball used in the measurements. The ball surface was generated using a set of low-order spherical harmonic functions.

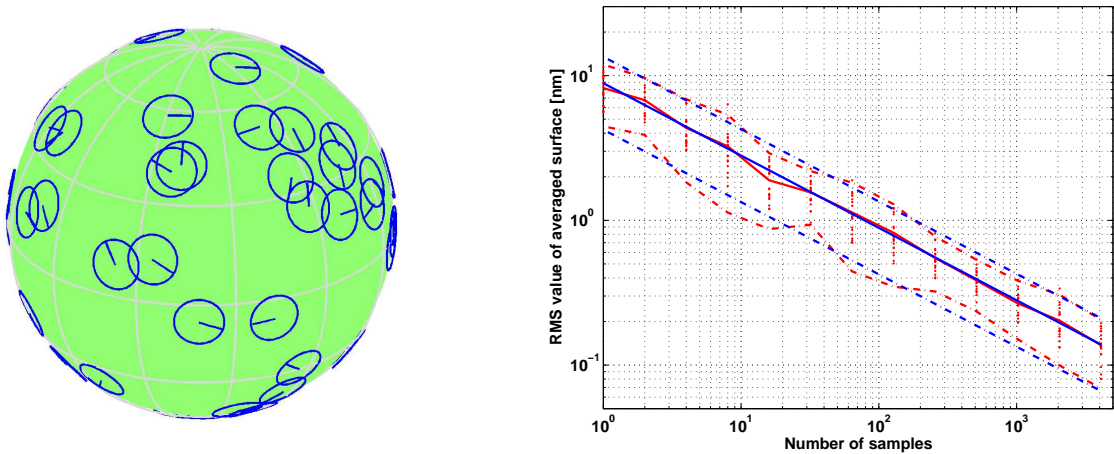


Figure 4. Random sampling strategy for the ball averaging test. The ball surface is sampled at random locations and the orientation of the measurement areas is chosen at random. Each circle indicates a measurement, for clarity shown with reduced size, whose orientation is indicated by the radial line. The actual measurement area corresponds to the area imaged with an interferometer objective having a numerical aperture of 0.39 ($f/1.3$). Note that both axes of the plot have logarithmic scales.

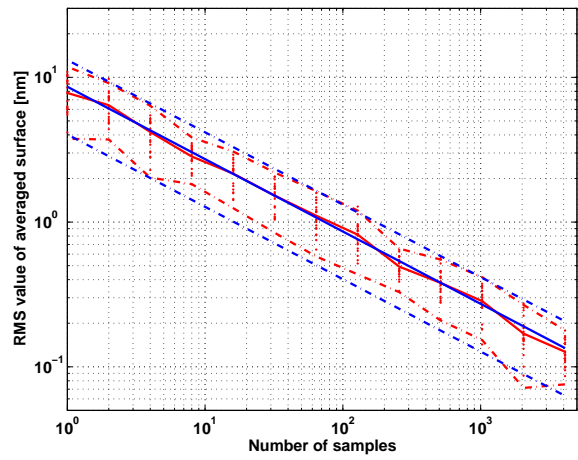
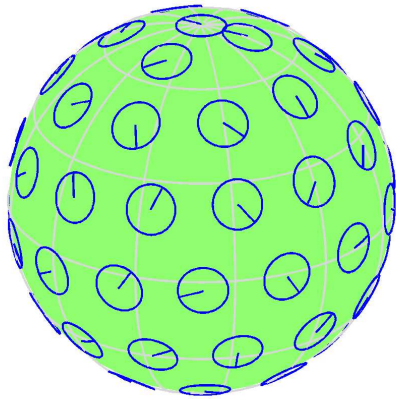


Figure 5. Uniform sampling strategy. The measurement locations have a nearly uniform density on the ball surface. The orientation of the measurement areas is also uniform. Every measurement location is assigned one of the orientations at random so that every location and every orientation occurs only once.

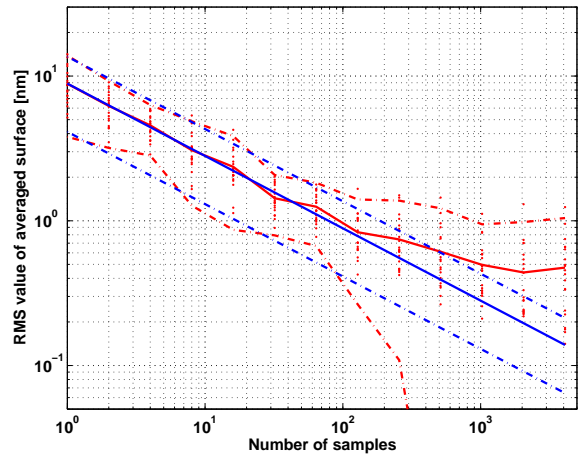
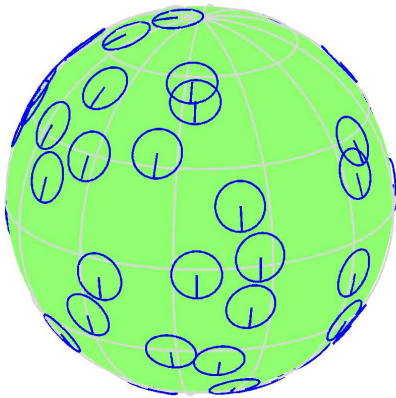


Figure 6. Random sampling without randomized orientation. The measurement locations are chosen at random as in Fig. 4 but the measurement orientation remains fixed.

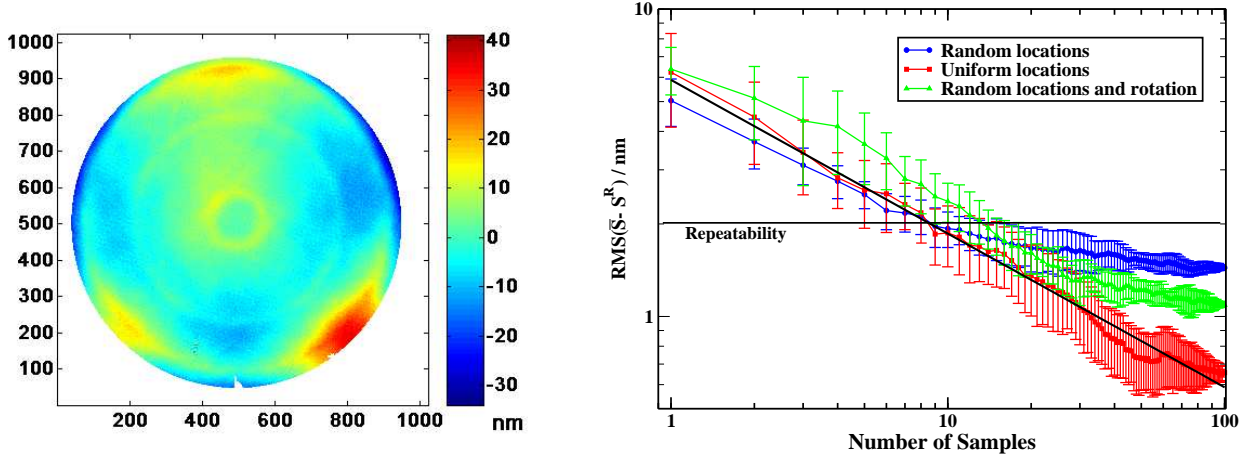


Figure 7. Reference wavefront of a NA=0.39 concave transmission sphere (left) and RMS of averaged measurements as function of the number of measurements for three different sampling strategies (right). The black line indicates the ideal $1/\sqrt{N}$ behavior. A horizontal black line indicates the measurement repeatability.

the computer simulation, the true reference wavefront is unknown which makes it more difficult to study the converging sum term on the right side of Eq. (3). Instead, the mean of the entire pool of measurements with all sampling strategies was used as an estimate for the reference surface $S^R = \frac{1}{2}W^R$. The plot in Fig. 7 shows the averaged measurements \bar{S} with the estimate for the reference wavefront subtracted. The order of the measurements was randomized 10 times and for each randomization \bar{S} was calculated as a function of N . The standard uncertainties of the resulting 10 values for \bar{S} are indicated with error bars in Fig. 7. The figure clearly shows how the second term in Equation (3) diminishes as more and more measurements are averaged. For small N the reduction in the calibration error is proportional to $1/\sqrt{N}$ as expected. For larger N the experimental curve deviates from the ideal $1/\sqrt{N}$ behavior. Because the true reference wavefront W^R is not known the graphs in Fig. 7 do not have the expected asymptotic behavior for large N . The value to which the graphs converge, $\text{RMS}(\bar{S} - S^R)$, is slightly different for each of the three sampling strategies.

We can now return to answering the question how many measurements are needed to calibrate the reference wavefront using the ball averaging test. When the measurement uncertainty of the interferometer, or at least the measurement repeatability, is known, Fig. 7 suggests a way to determine this number. For our XCALIBIR interferometer in spherical Fizeau configuration with a NA=0.39 (f/1.3) transmission sphere we have estimated the repeatability by making 9 measurements $S_i, i = 1 \dots 9$, of the black glass ball with one fixed orientation of the ball. Alignment errors, piston, tilts and defocus, were subtracted from each measurement. The average of all measurements was subtracted from the individual measurements and the RMS was calculated. The arithmetic mean of the RMS values, 2.0 nm, is a measure of the repeatability. This determines the number of measurements that must be averaged in the ball averaging test before the RMS of the averaged measurements drops below the repeatability. In the case of our measurement setup it appears that this point is reached after about 15 measurements where $\text{RMS}(\bar{S} - S^R)$ becomes significantly smaller than the measurement repeatability. When the measurement uncertainty is lower, and the horizontal black line in Fig. 7 moves down, more measurements will be required.

REFERENCES

1. A. E. Jensen, "Absolute calibration method for laser Twyman-Green wave-front testing interferometers," *J. Opt. Soc. Am.* **63**, p. 1313A, 1973.
2. G. Schulz and J. Schwider, "Interferometric testing of smooth surfaces," *Prog. Opt.* **13**, pp. 93–167, 1976.
3. B. E. Truax, "Absolute interferometric testing of spherical surfaces," in *Advances in Fabrication and Metrology for Optics and Large Optics, Proc. SPIE 966*, pp. 130–137, 1988.
4. J. E. Greivenkamp and J. H. Bruning, "Phase shifting interferometry," in *Optical Shop Testing, 2nd Edition*, D. Malacara, ed., pp. 577–580, Wiley, New York, 1992.
5. L. A. Selberg, "Absolute testing of spherical surfaces," in *Optical Fabrication and Testing Workshop, OSA Technical Digest Series 13*, pp. 181–184, 1994.
6. K.-E. Elssner, R. Burow, J. Grzanna, and R. Spolaczyk, "Absolute sphericity measurement," *Appl. Opt.* **28**, pp. 4649–4661, 1989.
7. R. E. Parks, C. J. Evans, and L. Shao, "Calibration of interferometer transmission spheres," in *Optical Fabrication and Testing Workshop, OSA Technical Digest Series 12*, pp. 80–83, 1998.
8. E. Weisstein, *Sphere point picking*, From MathWorld – A Wolfram Web Resource, <http://mathworld.wolfram.com/SpherePointPicking.html>, 2005.
9. E. B. Saff and A. B. J. Kuijlaars, "Distributing many points on a sphere," *The Mathematical Intelligencer* **19**, pp. 5–11, 1997.
10. C. J. Evans, M. Küchel, and C. A. Zanoni, "Apparatus and method for calibrating an interferometer using a selectively rotatable sphere. U.S. Patent 6,816,267," 2004.